



# Correlation between oxygen flow-controlled resistive switching and capacitance behavior in gallium oxide memristors grown via RF sputtering

Hye Jin Lee<sup>a</sup>, Jeong-Hyeon Kim<sup>a</sup>, Jongyun Choi<sup>a</sup>, Yoon Seok Kim<sup>b</sup>, Sung-Nam Lee<sup>a,b,\*</sup>

<sup>a</sup> Department of IT & Semiconductor Convergence Engineering, Tech University of Korea, Siheung, 15073, Republic of Korea

<sup>b</sup> Department of Nano & Semiconductor Engineering, Tech University of Korea, Siheung, 15073, Republic of Korea

## ARTICLE INFO

### Keywords:

Ga<sub>2</sub>O<sub>3</sub>  
Memristor  
Capacitance  
Oxygen vacancy  
RF sputter

## ABSTRACT

We studied on the bipolar resistive switching (RS)-dependent capacitance of Ga<sub>2</sub>O<sub>3</sub> memristors, grown using controlled oxygen flow via a radio frequency sputtering process. The Ag/Ga<sub>2</sub>O<sub>3</sub>/Pt memristor structure was employed to investigate the capacitance changes associated with RS behavior and oxygen concentration. In the low-resistance state (LRS), capacitance increased by over 60 times compared to the high-resistance state (HRS). Furthermore, in the HRS state, increasing the oxygen flow from 0 to 0.3 sccm resulted in an 80 % decrease in capacitance, while in the LRS state, capacitance increased by 128 %. These results indicate that RS-dependent capacitance in Ga<sub>2</sub>O<sub>3</sub> memristors is influenced by the density of oxygen vacancies. The presence of oxygen vacancies affects charge storage capacity and capacitance, with higher oxygen concentrations leading to reduced capacitance in HRS and increased capacitance in LRS. The results contribute to the understanding of the capacitance behavior in Ga<sub>2</sub>O<sub>3</sub> memristors and highlight the significance of oxygen vacancies in their operation.

## 1. Introduction

Ga<sub>2</sub>O<sub>3</sub> is highly regarded in electronic and optical devices due to its impressive properties, including a wide band gap of 4.9 eV, excellent physical and chemical characteristics, and thermal stability [1,2]. Consequently, it finds successful application in various optoelectronic uses, such as capacitors, photodetectors, gas sensors, and resistive memory [3–7]. In the field of resistive random-access memory (RRAM), Ga<sub>2</sub>O<sub>3</sub> has demonstrated remarkable potential. RRAM devices operate on the principle of resistive switching, allowing the resistance of a solid-state element to be altered between high-resistance state (HRS) and low-resistance state (LRS) [8]. Oxygen vacancies, which are intrinsic defects in Ga<sub>2</sub>O<sub>3</sub>, significantly impact the behavior and performance of RRAM devices by affecting channel formation, a crucial aspect of memristor operation [9,10]. The optimization of oxygen vacancy concentration becomes critical for enhancing the properties of Ga<sub>2</sub>O<sub>3</sub> RRAM. Researchers are actively investigating various aspects of Ga<sub>2</sub>O<sub>3</sub> RRAM technology, including characterizing Ga<sub>2</sub>O<sub>3</sub> properties like electrical conductivity, carrier concentration, and mobility [11–14]. Additionally, they focus on comprehending mechanisms underlying resistive switching, improving device performance, endurance,

\* Corresponding author. Department of IT & Semiconductor Convergence Engineering, Tech University of Korea, Siheung, 15073, Republic of Korea.

E-mail address: [snlee@tukorea.ac.kr](mailto:snlee@tukorea.ac.kr) (S.-N. Lee).

<https://doi.org/10.1016/j.heliyon.2023.e23157>

Received 20 July 2023; Received in revised form 21 November 2023; Accepted 28 November 2023

Available online 1 December 2023

2405-8440/© 2023 The Authors. Published by Elsevier Ltd. This is an open access article under the CC BY-NC-ND license (<http://creativecommons.org/licenses/by-nc-nd/4.0/>).

and scalability [15,16]. Many growth techniques to control and manipulate oxygen vacancies are also being explored [17]. Among these methods, the RF sputtering system stands out for growing  $\text{Ga}_2\text{O}_3$ , enabling the deposition of  $\text{Ga}_2\text{O}_3$  thin films with precise thickness and quality control [18]. The RF sputtering system enables precise control over deposition parameters, such as sputtering power, Ar/ $\text{O}_2$  gas pressure, and substrate temperature, ensuring reproducible growth of  $\text{Ga}_2\text{O}_3$  films with desired properties.

The intrinsic defects in  $\text{Ga}_2\text{O}_3$ , particularly oxygen vacancies, have a significant impact on the capacitance behavior of  $\text{Ga}_2\text{O}_3$  capacitors [19]. These defects play a crucial role in determining capacitance values and overall performance. Optimizing oxygen vacancy concentration is crucial for enhancing the capacitance properties of  $\text{Ga}_2\text{O}_3$  [20]. Its wide band gap and favorable dielectric properties make it well-suited for high-performance capacitors, capable of withstanding high electric fields with low leakage current [21]. These characteristics make  $\text{Ga}_2\text{O}_3$  capacitors desirable for applications requiring efficient energy storage and charge-discharge cycles. Furthermore, oxygen vacancies in  $\text{Ga}_2\text{O}_3$  have important implications for channel formation in memristor devices. The presence of oxygen vacancies influences ion migration and behavior during resistive switching, affecting the formation and dissolution of conductive channels [22,23]. Therefore, understanding and optimizing the concentration of oxygen vacancies are vital for achieving desirable memristor performance in  $\text{Ga}_2\text{O}_3$  devices. In this study, we investigated the relationship between the capacitance and resistance behavior of  $\text{Ga}_2\text{O}_3$  memristors grown using different oxygen flow rates in a radio frequency (RF) sputter. Furthermore, by measuring the capacitance values at HRS and LRS of  $\text{Ga}_2\text{O}_3$  memristors grown at different oxygen flow rates, we studied into the effect of oxygen vacancies on the capacitance response and resistance switching characteristics of memristor devices.

## 2. Materials and methods

The  $\text{Ga}_2\text{O}_3$  memristors were fabricated using RF sputtering on c-side sapphire substrates. Preceding the deposition, the substrates were cleaned using RCA cleaning method, involving sequential treatments with acetone, isopropyl alcohol, and deionized water to eliminate organic impurities. A 50 nm-thick bottom electrode of Pt was deposited on the cleaned sapphire substrates using RF sputtering. Subsequently, a  $\text{Ga}_2\text{O}_3$  thin film was deposited using RF sputtering with high-purity  $\text{Ga}_2\text{O}_3$  targets. This deposition process was carried out at room temperature, maintaining a base pressure of  $8.7 \times 10^{-7}$  Torr, a working pressure of  $3 \times 10^{-3}$  Torr, an RF power of 100 W. In addition, the oxygen flow rates were adjusted variably to regulate oxygen concentration within the  $\text{Ga}_2\text{O}_3$  thin film. The influence of oxygen concentration on  $\text{Ga}_2\text{O}_3$  thin films was studied by reducing the argon flow rate from 20 sccm to 19.7 sccm and progressively increasing the oxygen flow rate from 0 sccm to 0.3 sccm. This adjustment allowed us to manipulate the argon-to-oxygen flow ratio, resulting in ratios of 20:0 (0%), 19.9:0.1 (0.5%), 19.8:0.2 (1.0%), and 19.7:0.3 (1.5%). To complete the device structure, a 50 nm-thick top Ag electrode was deposited using a thermal evaporator.

To investigate the optical properties of the  $\text{Ga}_2\text{O}_3$  film, particularly its absorption behavior, a UV-visible spectrometer (ThermoFisher Scientific, Evolution 300) was employed. The optical band gap of the  $\text{Ga}_2\text{O}_3$  thin film was determined by measuring its optical absorbance in the UV-visible ranging from 200 nm to 800 nm. The X-ray photoelectron spectroscopy (XPS) spectra utilizing the ThermoFisher Scientific NEXSA system, were carefully analyzed to detect the presence of oxygen vacancies and to examine the chemical environment of the  $\text{Ga}_2\text{O}_3$  elements. The XPS spectra were calibrated to the standard C 1s peak at 284.8 eV. We conducted an in-depth analysis of the binding energy and peak intensity ratios of Ga 3d and O 1s to gain insight into changes in chemical states and the presence of defects within the  $\text{Ga}_2\text{O}_3$  film. For electrical characterization, including leakage current and memristor behavior, a Keithley 2614B source meter was used. The capacitance of the devices was characterized using a HP 4284A LCR meter, with frequency ranging from 500 Hz to 1 MHz. Through these experimental techniques and characterization methods, we investigated the relationship between the characteristics in the LRS and HRS and the capacitance of the  $\text{Ga}_2\text{O}_3$  memristors. Moreover, we analyzed the effect of

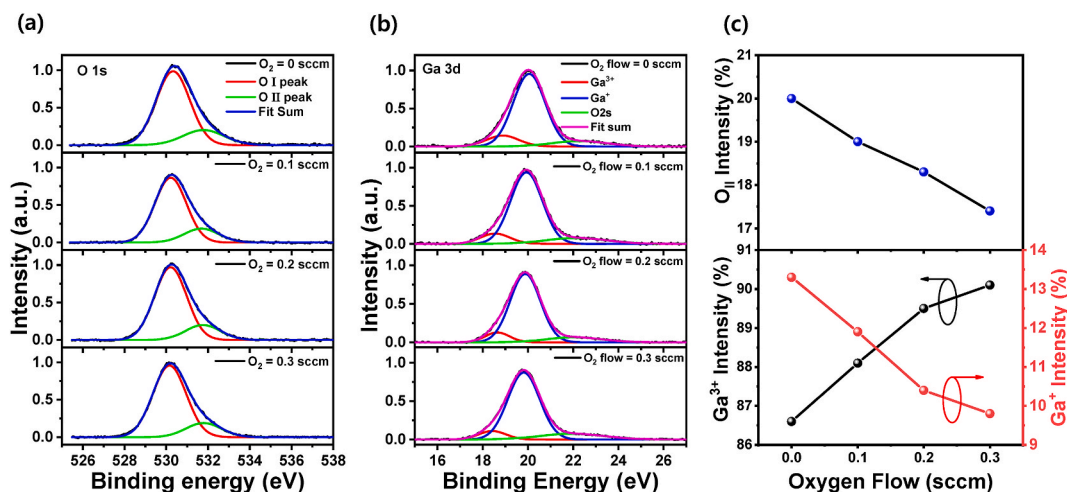


**Fig. 1.** XPS (a) O 1s and (b) Ga 3d peaks of  $\text{Ga}_2\text{O}_3$  film grown with different oxygen flow rates. (c) O<sub>II</sub>, Ga<sup>3+</sup> and Ga<sup>+</sup>-related peak intensity of  $\text{Ga}_2\text{O}_3$  film as a function of oxygen flow rate.

oxygen flow rate on their electrical behavior and performance of Ag/Ga<sub>2</sub>O<sub>3</sub>/Pt memristors.

### 3. Results and discussion

The chemical bonding states of Ga<sub>2</sub>O<sub>3</sub> films grown under different oxygen flow rates were investigated by XPS. In Fig. 1 (a), the O 1s peaks of Ga<sub>2</sub>O<sub>3</sub> films reveal two distinct peaks. The first peak, labeled as O<sub>I</sub>, appears at a low binding energy of 530 eV and corresponds to O<sup>2-</sup> ions surrounded by Ga atom. The second peak, denoted as O<sub>II</sub>, appears at a higher energy of 531.8 eV and is associated with oxygen vacancies within the metal bonding matrix [24]. The ratio of the area under the O<sub>II</sub> peak to the total area under the O 1s peak (O<sub>I</sub> + O<sub>II</sub>) provides a measure of the relative quantity of oxygen vacancy-related peak area ratio, which decreased from 20 % to 17.4 %, as shown in Fig. 1 (c). This indicates that increasing the oxygen flow during RF sputtering reduces the concentration of oxygen vacancies in the Ga<sub>2</sub>O<sub>3</sub> films [25]. Fig. 1 (b) illustrates the Ga 3d peaks observed in the Ga<sub>2</sub>O<sub>3</sub> films with different oxygen flow rates. These peaks comprise O 2s, Ga 3d (Ga<sup>3+</sup>), and Ga 3d (Ga<sup>1+</sup>). The Ga 3d peak can be decomposed into Ga<sup>3+</sup> and Ga<sup>1+</sup> peaks, corresponding to binding energies of 20.0 eV and 18.5 eV, respectively [26]. Ga<sup>3+</sup> represents the lattice component of Ga<sub>2</sub>O<sub>3</sub>, while Ga<sup>1+</sup> corresponds to the Ga<sub>2</sub>O phases [27]. When the oxygen flow rate increases from 0 sccm to 0.3 sccm, the Ga<sup>3+</sup> peak intensity increases from 86.6 % to 90.1 %, whereas the Ga<sup>1+</sup> peak intensity decreases from 13.3 % to 9.8 %, as shown in Fig. 1(c). This indicates that increasing the oxygen flow rate promotes the growth of the Ga<sub>2</sub>O<sub>3</sub> phase at the expense of the Ga<sub>2</sub>O phase [28]. Based on these results, it is believed that increasing the oxygen flow rate can improve the quality of the Ga<sub>2</sub>O<sub>3</sub> film by reducing oxygen vacancies and favoring the formation of the Ga<sub>2</sub>O<sub>3</sub> phase.

Fig. 2 (a) shows the optical absorption spectra of Ga<sub>2</sub>O<sub>3</sub> films grown under different oxygen flow rates, ranging from 0 sccm to 0.3 sccm. The energy bandgap of Ga<sub>2</sub>O<sub>3</sub> films with varying oxygen flow rates can be determined using the equation  $\alpha h\nu = B(h\nu - E_g)^{1/2}$ , where  $\alpha$  is the absorption coefficient,  $h$  is the Planck constant ( $4.135 \times 10^{-15}$  eVs),  $\nu$  denotes the frequency ( $s^{-1}$ ),  $B$  is a constant, and  $E_g$  represents the energy band gap (eV) [29]. The bandgap energy can be calculated by extrapolating the linear portion of the curve to the energy axis. In Fig. 2 (a), the optical absorption spectra demonstrate the relationship between the absorption coefficient and energy for Ga<sub>2</sub>O<sub>3</sub> films at different photon energies. Notably, there is an increasing trend in the optical bandgap of Ga<sub>2</sub>O<sub>3</sub> films with an increase in the oxygen flow rate. Fig. 2 (b) illustrates the optical bandgap values for Ga<sub>2</sub>O<sub>3</sub> films grown under different oxygen flow rates, ranging from 0 sccm to 0.3 sccm. The measured bandgap values were found to be 4.808 eV for films grown at an oxygen flow rate of 0 sccm and 4.907 eV for films grown at an oxygen flow rate of 0.3 sccm. This observed change in the bandgap can be attributed to the supplement of oxygen during the deposition of Ga<sub>2</sub>O<sub>3</sub> films. The introduction of additional oxygen during the deposition process reduces the presence of oxygen vacancies and promotes the formation of Ga<sub>2</sub>O<sub>3</sub>, as depicted in Fig. 2. This adjustment enables the achievement of the ideal atomic ratio, leading to an enhancement in the crystal quality of the Ga<sub>2</sub>O<sub>3</sub> thin film [30]. The concentration and distribution of oxygen vacancies within the Ga<sub>2</sub>O<sub>3</sub> crystal lattice play a significant role in the energy bandgap. Higher concentrations of oxygen vacancies can introduce localized states within the bandgap, resulting in a decrease in the effective bandgap energy. Conversely, lower concentrations or effective control of oxygen vacancies can help maintain or enhance the bandgap energy of Ga<sub>2</sub>O<sub>3</sub> [19]. Therefore, it is believed that increasing the oxygen flow during deposition decreases the concentration of oxygen vacancies in Ga<sub>2</sub>O<sub>3</sub>, ultimately resulting in higher crystal quality in the Ga<sub>2</sub>O<sub>3</sub>.

To evaluate the effect of oxygen flow on Ga<sub>2</sub>O<sub>3</sub> film growth using RF sputtering, the current – voltage (*I* – *V*) curves were measured for Ag/Ga<sub>2</sub>O<sub>3</sub>/Pt memristor structure, as shown in Fig. 3 (a). Fig. 3 (b) illustrates the leakage current behaviors of Ga<sub>2</sub>O<sub>3</sub> resistive switching (RS) memristor structures grown with different oxygen flow rates, under applied biases ranging from –1.0 V to +1.0 V. It indicates that, as the oxygen flow rate increases from 0 sccm to 0.3 sccm, the leakage current progressively decreases from 6.24  $\mu$ A to 32.5 pA at an applied voltage of 1.0 V. This reduction in leakage current can be attributed to the diminished presence of defects, such as oxygen vacancies, in the Ga<sub>2</sub>O<sub>3</sub> thin film grown with the introduction of additional oxygen gas during deposition [31]. By controlling

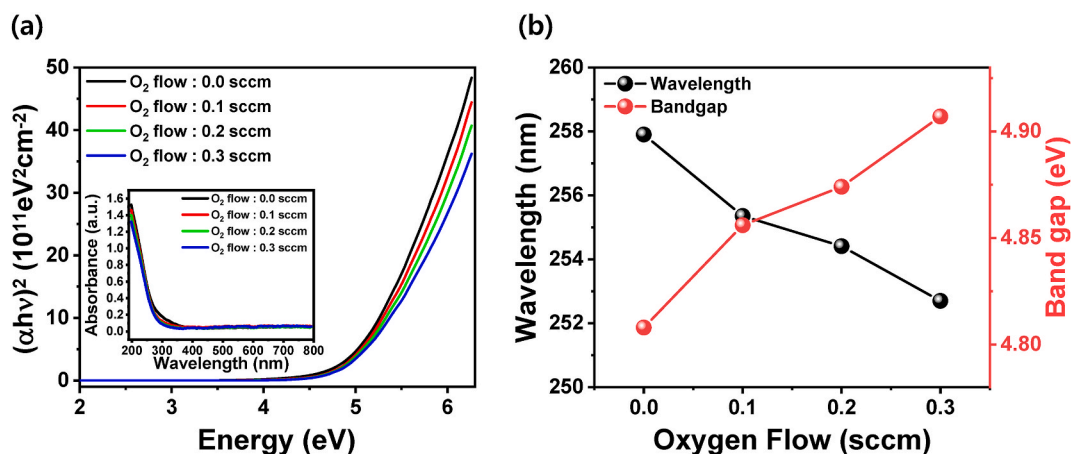
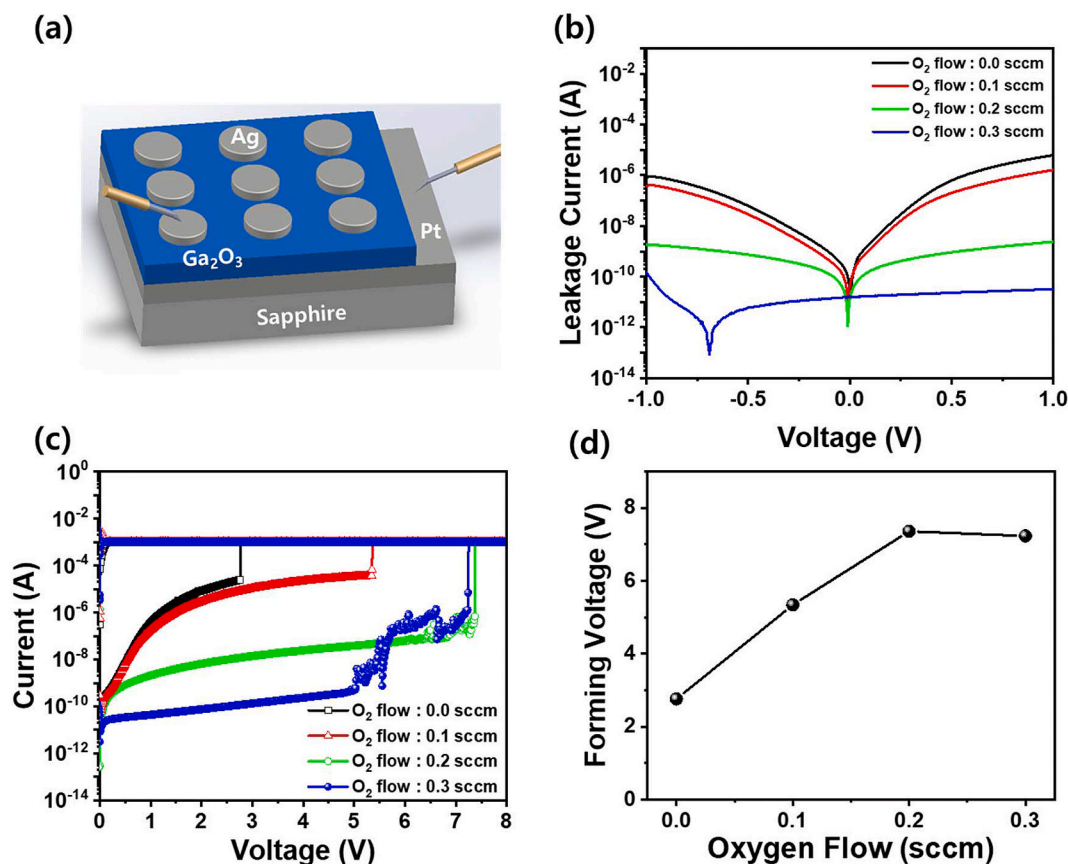


Fig. 2. (a) Plot of  $(\alpha h\nu)^2$  against *E* for the Ga<sub>2</sub>O<sub>3</sub> films with different oxygen flow. Inset is the absorbance spectra of the same films. (b) Energy bandgap of Ga<sub>2</sub>O<sub>3</sub> films grown by different oxygen flow rates ranging from 0 sccm to 0.3 sccm in RF sputter.



**Fig. 3.** (a) Schematic diagram of Ag/Ga<sub>2</sub>O<sub>3</sub>/Pt memristor, (b) I–V curves for measuring leakage current before the forming process, and (c) I–V curves for the forming process to achieve the LRS in Ag/Ga<sub>2</sub>O<sub>3</sub>/Pt memristors grown with varying oxygen flow rates. (d) The forming voltage of Ag/Ga<sub>2</sub>O<sub>3</sub>/Pt memristors as a function of oxygen flow rates.

the oxygen flow during the deposition of the Ga<sub>2</sub>O<sub>3</sub> thin film, we enhance its insulating properties, resulting in lower operating currents in the HRS of the Ga<sub>2</sub>O<sub>3</sub> RS layer-embedded memristor device. In Ag/Ga<sub>2</sub>O<sub>3</sub>/Pt memristors, the current flow is significantly affected by the presence of oxygen vacancies, Ag<sup>+</sup> and O<sup>2-</sup> ions [32,33]. The shift in voltage associated with the minimum current appears to be driven by the existence of an internal electric field within the Ga<sub>2</sub>O<sub>3</sub> cell, dependent voltage polarization [34]. This effect likely arises from the differential mobility of Ag<sup>+</sup> and O<sup>2-</sup> ions in response to changes in the applied voltage. Ga<sub>2</sub>O<sub>3</sub> films grown with low oxygen flow rates exhibit relatively high levels of oxygen vacancies, resulting in an increased leakage current, as shown in Fig. 3 (b). These abundant oxygen vacancies facilitate the uniform distribution of Ag<sup>+</sup> and O<sup>2-</sup> ions through the vacancies, leading to symmetric I–V curves at 0 V bias. However, with a high oxygen flow rate (0.3 sccm), the oxygen vacancy concentration is comparatively lower compared to other samples. This leads to a significantly reduced migration rate of Ag<sup>+</sup> and O<sup>2-</sup> ions, resulting in an extremely low leakage current below 10<sup>-10</sup> A. Moreover, when a forward bias is applied to the Ag electrode from –1.0 V to +1.0 V, Ag<sup>+</sup> and O<sup>2-</sup> ions migrate to the Ag (–) and Pt (+) electrodes, respectively. As a result, a minimum current is formed at –0.7 V, where the depletion of Ag<sup>+</sup> and O<sup>2-</sup> ions as conductive sources within the Ga<sub>2</sub>O<sub>3</sub> film is maximized, as illustrated in the previous Fig. 3 (b). Similarly, it is observed that a minimum current of +0.75 V is obtained when a reverse bias is applied to the Ag electrode from +1.0 V to –1.0 V. This finding provides clear evidence of an internal electric field within the Ga<sub>2</sub>O<sub>3</sub> material grown with a high oxygen flow rate. Fig. 3 (c) displays the I–V characteristics of the Ga<sub>2</sub>O<sub>3</sub> memristor grown with varying oxygen flow rates. The behavior of Ga<sub>2</sub>O<sub>3</sub> memristor is observed by applying an increasing voltage from 0 V to 8.0 V and then decrease it back to 0 V. In memristor devices, the “forming voltage” refers to the voltage at which a transition from a HRS transition to a LRS occurs during the initial operation. During the forming process, a high current flows through the device, typically in the range of mA or higher. This is due to the establishment of a conductive filament which involves the migration and diffusion of oxygen vacancies and mobile ions, such as Ag<sup>+</sup> and O<sup>2-</sup> ions, from the electrode interfaces into the Ga<sub>2</sub>O<sub>3</sub> material [32]. The formation of these conductive filaments is achieved by applying a voltage from 0 V to 8.0 V, followed by a return to 0 V. It is observed that as the oxygen flow rate increases from 0 sccm to 0.3 sccm, the forming voltage increases rapidly from 2.8 V to 7.2 V, respectively. This phenomenon can be attributed to the reduced number of oxygen vacancies present in the Ga<sub>2</sub>O<sub>3</sub> thin films. Oxygen vacancies play a crucial role in the formation of the conductive filament within the memristor device [32,33]. When the oxygen flow is increased, such as an oxygen flow of 0.3 sccm resulting in fewer oxygen vacancies, the device requires higher voltages to initiate the switching process.

Fig. 4(a–d) illustrates the RS behaviors of bipolar Ag/Ga<sub>2</sub>O<sub>3</sub>/Pt memristors grown with different oxygen flow rates of 0, 0.1, 0.2 and 0.3 sccm, respectively. The RS curves were obtained by applying a sequence of four input bias steps: 0 V–5.0 V, 5.0 V–0 V, 0 V to –3.0 V, and –3.0 V–0 V. In the first step (0 V–5.0 V), known as the “set” process, a voltage is applied from 0 V to 5.0 V, which facilitates the formation of a conductive filament responsible for the LRS of the device. As shown in Fig. 3 (d), it is observed that the forming voltage increases rapidly from 2.8 V to 7.2 V with an increase in oxygen flow from 0 sccm to 0.3 sccm. However, after the “forming” process of the Ga<sub>2</sub>O<sub>3</sub> memristor, it is found that the set and reset voltages increase from 1.63 V to 3.36 V and from –1.10 V to –1.52 V, respectively, as the oxygen flow rate increases from 0 sccm to 0.3 sccm, as shown in Fig. 4 (e) and (f). In general, conductive filaments in metal/Ga<sub>2</sub>O<sub>3</sub>/metal memristors are known to form via oxygen vacancy and metal ion migration [32,33]. When using a noble metal like Pt, the primary conduction mechanism in oxide memristor involves the electrical field-induced migration of oxygen vacancies [20, 23]. In contrast, with an active metal electrode like Ag, the formation of conductive filaments relies on Ag<sup>+</sup>, O<sup>2-</sup> ions and oxygen vacancies [32,33,35]. From the XPS results shown in Fig. 1 (a) and (b), the increase of the oxygen flow rate leads to a reduction in oxygen vacancies in Ga<sub>2</sub>O<sub>3</sub> films, favoring the dominance of Ga<sub>2</sub>O<sub>3</sub> over Ga<sub>2</sub>O. Furthermore, as the oxygen flow rate increases from 0 sccm to 0.3 sccm, the leakage current in Ag/Ga<sub>2</sub>O<sub>3</sub>/Pt memristors decreases, while the forming voltage required to achieve a LRS increases. This behavior can be attributed to the decreased presence of oxygen vacancies, emphasizing their role in conductive channel formation in Ag/Ga<sub>2</sub>O<sub>3</sub>/Pt memristors. Additionally, it is observed that the set voltage of Pt/Ga<sub>2</sub>O<sub>3</sub>/Pt memristor is approximately three times higher than that of Ag/Ga<sub>2</sub>O<sub>3</sub>/Pt memristor, as illustrated in Fig. 4(a) and its inset. This difference suggests that oxygen vacancies, rather than metal ions, mainly contributed to the formation of conductive channels in Pt/Ga<sub>2</sub>O<sub>3</sub>/Pt memristor due to the inert nature of noble Pt metal. In contrast, in Ag/Ga<sub>2</sub>O<sub>3</sub>/Pt memristor, the process is significantly influenced by both oxygen vacancies and Ag<sup>+</sup> ions. Therefore, the formation mechanism of conductive channel in Ag/Ga<sub>2</sub>O<sub>3</sub>/Pt memristors is believed to involve both Ag<sup>+</sup> ions and oxygen vacancies, making it easier to form these channels at lower voltages compared to Pt/Ga<sub>2</sub>O<sub>3</sub>/Pt memristors, as shown in Fig. 4 (g) [32,33]. Similar to the increase in the forming voltage, it has also been observed that the “set” voltage of the Ga<sub>2</sub>O<sub>3</sub> memristors increases with higher oxygen flow rate during Ga<sub>2</sub>O<sub>3</sub> growth. This observation suggests that a higher oxygen flow reduces the presence of oxygen vacancies, making it more difficult for conductive filaments to form [36]. Consequently, a higher voltage is required to induce the switching to the LRS. Furthermore, an increase in the oxygen flow rate during Ga<sub>2</sub>O<sub>3</sub> growth results in an increase from  $4.6 \times 10^5$  to  $3.6 \times 10^6$  in the offset current in the Ga<sub>2</sub>O<sub>3</sub> memristor, which represents the difference between the operating current in the HRS and LRS before and after the set voltage, as shown in Fig. 4 (h–k). This can be attributed to the reduction of defects, such as oxygen vacancies, in the HRS as the oxygen flow rate increases. Therefore, the lower current in the HRS leads to a larger offset current between the HRS and LRS, indicating an improvement in memory characteristics. A larger offset current provides a

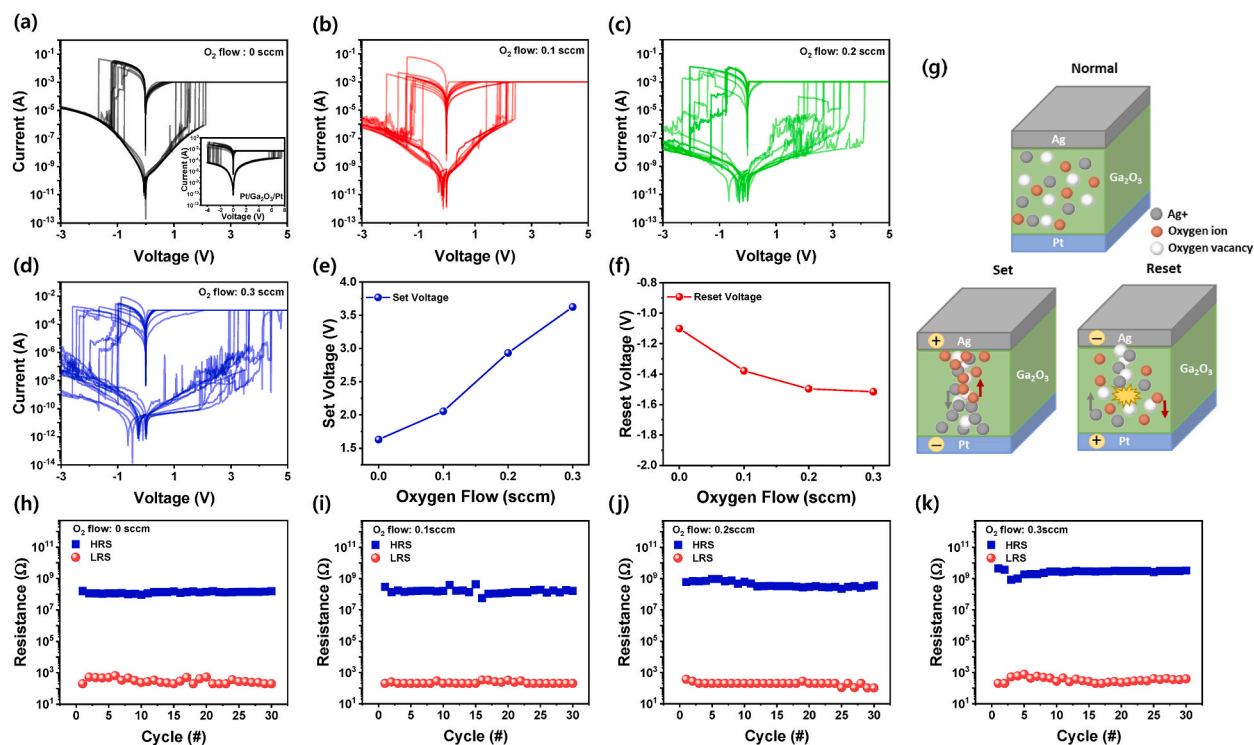


Fig. 4. RS behaviors of I–V curves for Ag/Ga<sub>2</sub>O<sub>3</sub>/Pt memristor with different oxygen flow of (a) 0 sccm, (b) 0.1 sccm, (c) 0.2 sccm, and (d) 0.3 sccm. The (e) set and (f) reset voltages of memristors as a function of oxygen flow rates. Voltage offsets between HRS and LRS for Ga<sub>2</sub>O<sub>3</sub> memristors grown with oxygen flow rates of (h) 0 sccm, (i) 0.1 sccm, (j) 0.2 sccm, and (k) 0.3 sccm. (g) The schematic diagram of the set and reset processes for Ag/Ga<sub>2</sub>O<sub>3</sub>/Pt memristor.

more distinct differentiation between the two resistance states, enabling a more reliable and robust operation of the memristor device [37]. To ensure device stability and prevent breakdown while allowing the formation of a large conductive channel, specific compliance currents are set [38]. The forward compliance current is limited to 1.0 mA, while the reverse compliance current is set at 100 mA. These compliance currents act as safety measures to control the current flowing through the device. In the sequential bias step, the second step involves reducing the applied voltage to 0 V, effectively returning the device to its initial state. The third step, known as the “reset” process, involves applying a reverse voltage from 0 V to  $-3.0$  V. This reverse voltage causes the elimination or disruption of the conductive filament, resulting in a HRS in the device. In the fourth step, the applied voltage is restored to 0 V, completing the reset process and returning the device to its initial state. During the “reset” process, a slight increase in the reset voltage of the  $\text{Ga}_2\text{O}_3$  memristor was observed, ranging from  $-1.10$  V to  $-1.52$  V, as the oxygen flow rate increased from 0 sccm to 0.3 sccm. This indicates that the increase in the reset voltage is relatively small compared to the change observed in the set voltage with increasing oxygen flow rate. These findings suggest that the presence of oxygen vacancies may not have a direct and significant influence on the removal of an already formed conductive filament in the  $\text{Ga}_2\text{O}_3$  memristor [39]. Furthermore, the reset voltage exhibits minimal variation with increasing oxygen flow in the  $\text{Ga}_2\text{O}_3$  memristor, remaining relatively stable regardless of the oxygen flow rate. In the set process, a conductive filament is formed through the migration of oxygen vacancies and  $\text{Ag}^+$  ions, leading to the LRS. However, during the reset process under reverse bias, the reset voltage is lower than the set voltage due to the easier migration of  $\text{Ag}^+$  ions compared to oxygen vacancies [40]. Moreover, a higher voltage is not required because the  $\text{Ag}^+$  ions migrate more actively within the presence of oxygen vacancies and other  $\text{Ag}^+$  ions [41]. However, it is still believed that a device with a high oxygen flow rate will have a slightly higher reset voltage due to the difficulty in migrating  $\text{Ag}^+$  ions due to fewer oxygen vacancies.

The effect of conductive filament formation on the capacitance of the  $\text{Ga}_2\text{O}_3$  RS memristor was investigated by measuring capacitance values in the LRS and HRS states. Fig. 5 (a), (b), and (c) show the capacitance of  $\text{Ag}/\text{Ga}_2\text{O}_3/\text{Pt}$  memristors grown with different oxygen flow rates for  $\text{Ga}_2\text{O}_3$ , as a function of the applied bias ranging from  $-0.5$  V to  $+0.5$  V. In the initial HRS, the capacitance of the  $\text{Ga}_2\text{O}_3$  memristor decreases with increasing oxygen flow, as shown in Fig. 5 (a). This decrease in capacitance can be attributed to a reduction in defects, such as oxygen vacancies, which occur with higher oxygen flow rates during  $\text{Ga}_2\text{O}_3$  growth. High resistivity in the dielectric material limits the ability to accumulate charges, resulting in lower capacitance even with low leakage current [42]. Defects, impurities, or trap sites within the dielectric material can also affect charge distribution and result in higher

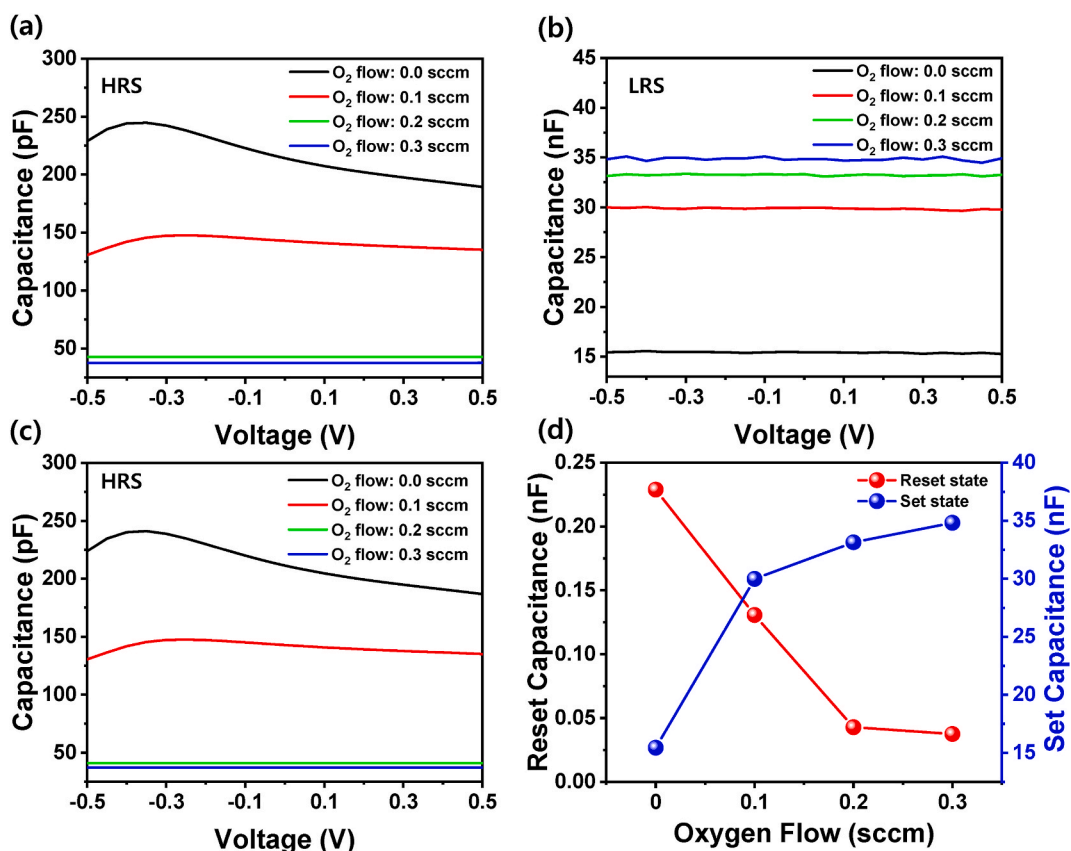


Fig. 5. Capacitance – voltage ( $C-V$ ) curves of  $\text{Ag}/\text{Ga}_2\text{O}_3/\text{Pt}$  memristor with varying oxygen flow in (a) the initial HRS, (b) the LRS after switching from initial HRS, and (c) the HRS after transitioning from LRS as a function of applied voltage. (d) The capacitance in the set and reset of the  $\text{Ag}/\text{Ga}_2\text{O}_3/\text{Pt}$  memristor as a function of the oxygen flow rates.

capacitance. These defects can influence the movement and trapping of charges, increasing the effective capacitance despite high leakage current [43]. In the LRS, all samples exhibit a significant increase in capacitance, exceeding 10 times, ranging from sub-nA levels to 15–34 nA, as depicted in Fig. 5(a) and (b). This increase in capacitance under LRS is observed regardless of the oxygen flow rate during Ga<sub>2</sub>O<sub>3</sub> growth. It suggests that more carriers are effectively supplied from the electrode to the Ga<sub>2</sub>O<sub>3</sub> layer through the formation of a conductive filament. The conductive filament, formed by the migration of Ag<sup>+</sup> ions and oxygen vacancies, acts as a pathway for charge transport within the Ga<sub>2</sub>O<sub>3</sub> memristor [35]. Consequently, more charges can be stored in the conductive filament, leading to the higher charge storage capacity observed in the LRS [44]. Furthermore, when the memristor transitions back to the HRS through the reset process, the capacitance exhibits a behavior similar to the initial HRS state, as shown in Fig. 5 (c). This indicates that the capacitance values return to a level comparable to the initial HRS after the conductive filament is dissolved during the reset process. In addition, in the HRS, as the oxygen flow rate increases from 0 sccm to 0.3 sccm, the reset capacitance at 0.5 V tends to decrease from 0.238 nF to 0.037 nF, as shown in Fig. 5 (d). A higher concentration of defects, such as oxygen vacancies, in the Ga<sub>2</sub>O<sub>3</sub> RS layer at the oxygen flow rate of 0 sccm results in more leakage paths but provides the available area for storing more charge, leading to a larger capacitance value. In contrast, in the LRS, as the oxygen flow rate increases from 0 sccm to 0.3 sccm, the set capacitance tends to increase from 15.3 nF to 34.9 nF at 0.5 V, respectively. The migration of Ag<sup>+</sup> ions during the channel formation process can contribute to the increased capacitance in the LRS [45]. Higher oxygen flow rates reduce the oxygen vacancy concentration in the Ga<sub>2</sub>O<sub>3</sub> RS layer, as shown in Fig. 1 (a). Therefore, when forming a channel, additional charge such as Ag<sup>+</sup> ions move into the RS layer and enhance the polarization phenomenon in LRS, resulting in increased capacitance [46]. Conversely, when transitioning from the LRS to the HRS, the migration of oxygen vacancies back into other regions of the Ga<sub>2</sub>O<sub>3</sub> layer interfaces with polarization formation, leading to lower capacitance in the HRS. The migration and redistribution of oxygen vacancies play a crucial role in the observed capacitance changes during the transition between LRS and HRS in the Ga<sub>2</sub>O<sub>3</sub> memristor.

Fig. 6 (a) shows an analysis of the resistive memory characteristics through voltage sweeping C – V with hysteresis. Upon repeated application of voltage for set and reset processes across all samples, hysteresis is observed in the C – V curves, irrespective of the oxygen flow rate. Increasing the oxygen flow rate is found to result in higher set and reset voltages. In particular, the set voltage, which correlated with an increase in capacitance, shows higher values with an increased oxygen flow rate. Similarly, the reset voltage, associated with a decrease in capacitance, also exhibits an increase with higher oxygen flow rate. Furthermore, the maximum capacitance achieved after the set process increases from 25 nF to 65 nF as the oxygen flow rate increases. This indicates that a higher oxygen flow rate during Ga<sub>2</sub>O<sub>3</sub> growth has a positive impact on the capacitance of the memristor, potentially leading to enhanced charge storage capacity and improved device performance [47]. These observed hysteresis in capacitance and the increase in maximum capacitance highlight the effect of oxygen flow rate on the electrical behavior and performance of the Ga<sub>2</sub>O<sub>3</sub> memristor. In addition, to calculate the charge trapping density of the Ga<sub>2</sub>O<sub>3</sub> memristor with different oxygen flow rates, the following equation is used:

$$N_{\text{charge}} = \frac{\Delta VC_{\text{LRS}}}{qA}$$

where  $\Delta V$  is the difference between the set voltage and reset voltage, and  $C_{\text{LRS}}$  is the capacitance in the LRS,  $q$  is the electronic charge ( $1.602 \times 10^{-19}$  C), and  $A$  is the area of the device [48]. Calculating the charge trapping density provides information about the density of trapped charges in the device, which is directly related to the charge storage capability and performance of the memristor. The  $\Delta V$  of hysteresis increases as the oxygen flow rate increases. For oxygen flow rates of 0 sccm, 0.1 sccm, 0.2 sccm and 0.3 sccm, the  $\Delta V$  values reach 9.0 V, 9.5 V, 12.0 V, and 13.2 V, respectively. Moreover, as shown in Fig. 6 (b), the  $N_{\text{charge}}$  values, which represent the

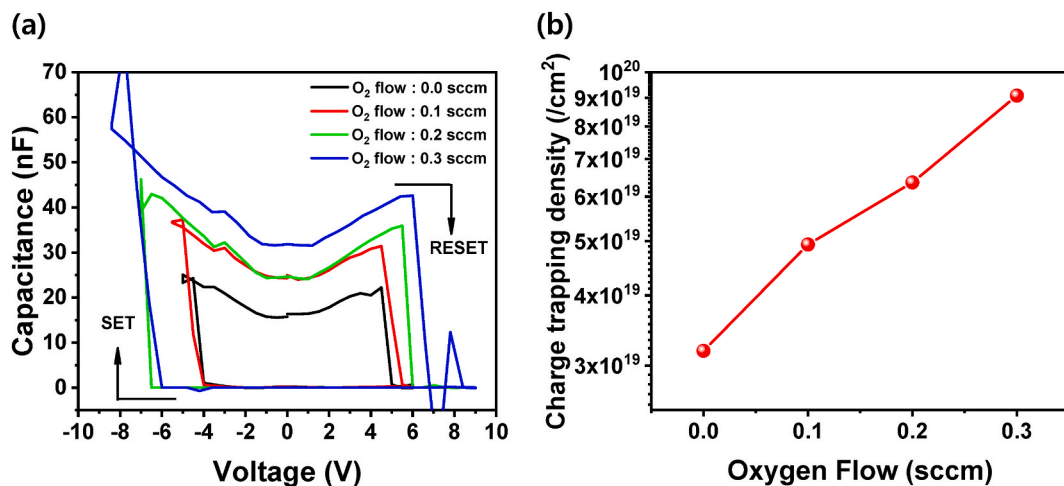


Fig. 6. (a) C – V hysteresis characteristics of the Ag/Ga<sub>2</sub>O<sub>3</sub>/Pt memristor grown with different oxygen flow rates during the resistive switching process and (b) the charge trapping density of the Ag/Ga<sub>2</sub>O<sub>3</sub>/Pt memristor as a function of the oxygen flow rates.

charge trapping density, also increase from  $3.19 \times 10^{19} \text{ cm}^{-2}$  to  $9.08 \times 10^{19} \text{ cm}^{-2}$  with the increase in oxygen flow rate from 0 sccm to 0.3 sccm, respectively. The observed increase in  $N_{\text{charge}}$  values, corresponding to the charge trap density, suggests that the movement of  $\text{Ag}^+$  ions is facilitated through defect sites within the  $\text{Ga}_2\text{O}_3$  layer, resulting in their trapping within the defective regions. This phenomenon of  $\text{Ag}^+$  ion trapping significantly influences the charge storage capacity and affects the resistive switching behavior of the memristor [49]. The higher  $N_{\text{charge}}$  values indicate a greater density of trapped charges, signifying an enhanced charge storage capability and holding the potential for improved device performance.

#### 4. Conclusions

The comprehensive analysis of  $\text{Ga}_2\text{O}_3$  memristors reveals a strong correlation between the characteristics of the LRS and HRS and the capacitance, which is influenced by the oxygen flow rate during growth. By increasing the oxygen flow rate, we observed a decrease in the concentration of oxygen vacancies, leading to significant improvements in LRS characteristics. XPS analysis further corroborates the reduction in oxygen vacancies with increasing oxygen flow rate. The migration of  $\text{Ag}^+$  ions and oxygen vacancies play a crucial role in forming a conductive filament, acting as a pathway for charge transport within the memristor. This conductive filament enables the efficient supply of carriers from the electrode to the  $\text{Ga}_2\text{O}_3$  layer, resulting in higher charge storage capacity and an overall increase in capacitance in the LRS. Additionally, the observed hysteresis in capacitance and the increase in maximum capacitance highlight the influence of the oxygen flow rate on the electrical behavior and performance of  $\text{Ga}_2\text{O}_3$  memristors. These findings provide valuable insights for optimizing device design and improving the performance of  $\text{Ga}_2\text{O}_3$ -based memristor devices. Overall, our study demonstrates the significance of oxygen vacancies and their control through the oxygen flow rate in shaping the LRS and HRS characteristics and capacitance of  $\text{Ga}_2\text{O}_3$  memristors.

#### Data availability

The data used to support the findings of this study can be made available by the corresponding author upon request.

#### CRediT authorship contribution statement

**Hye Jin Lee:** Writing – original draft, Methodology, Formal analysis, Data curation. **Jeong-Hyeon Kim:** Methodology, Investigation, Data curation. **Jongyun Choi:** Methodology, Investigation. **Yoon Seok Kim:** Validation, Methodology. **Sung-Nam Lee:** Writing – review & editing, Visualization, Supervision, Project administration, Funding acquisition, Conceptualization.

#### Declaration of competing interest

The authors declare the following financial interests/personal relationships which may be considered as potential competing interests.

#### Acknowledgements

This work was supported by project for Collabo R&D between Industry, University, and Research Institute funded by Korea Ministry of SMEs and Startups in 2023 (RS-2023-00225079) and by Research Programs (NRF-2020R1A2C1009630) through the National Research Foundation (NRF) of Korea, funded by the Ministry of Education, Science and Technology, Republic of Korea.

#### References

- [1] S. Ohira, N. Arai, T. Oshima, S. Fujita, Atomically controlled surfaces with step and terrace of  $\beta\text{-Ga}_2\text{O}_3$  single crystal substrates for thin film growth, *Appl. Surf. Sci.* 254 (2008) 7838–7842, <https://doi.org/10.1016/j.apsusc.2008.02.184>.
- [2] M. Orita, H. Ohta, M. Hirano, H. Hosono, Deep-ultraviolet transparent conductive  $\beta\text{-Ga}_2\text{O}_3$  thin films, *Appl. Phys. Lett.* 77 (2000) 4166–4168, <https://doi.org/10.1063/1.1330559>.
- [3] M. Passlack, E.F. Schubert, W.S. Hobson, M. Hong, N. Moriya, S.N.G. Chu, K. Konstadinidis, J.P. Mannaerts, M.L. Schnoes, G.J. Zydzik,  $\text{Ga}_2\text{O}_3$  films for electronic and optoelectronic applications, *Appl. Phys. Lett.* 77 (1995) 686–693, <https://doi.org/10.1063/1.359055>.
- [4] K.H. Shiu, T.H. Chiang, P. Chang, L.T. Tung, M. Hon, J. Kwo, W. Tsai, 1 nm equivalent oxide thickness in  $\text{Ga}_2\text{O}_3$  ( $\text{Ga}_2\text{O}_3$ ) / in 0.2 Ga 0.8 as metal-oxide semiconductor capacitors, *Appl. Phys. Lett.* 92 (2008), 172904, <https://doi.org/10.1063/1.2918835>. –1–172904–4.
- [5] R. Suzuki, S. Nakagomi, Y. Kokubun, N. Arai, S. Ohira, Enhancement of responsivity in solar-blind  $\beta\text{-Ga}_2\text{O}_3$  photodiodes with a Au Schottky contact fabricated on single crystal substrates by annealing, *Appl. Phys. Lett.* 94 (2009), 222102, <https://doi.org/10.1063/1.3147197>. –1–222102–4.
- [6] M. Ogita, K. Higo, Y. Nakanishi, Y. Hatanaka,  $\text{Ga}_2\text{O}_3$  thin film for oxygen sensor at high temperature, *Appl. Surf. Sci.* 175 (2001) 721–725, [https://doi.org/10.1016/S0169-4332\(01\)00080-0](https://doi.org/10.1016/S0169-4332(01)00080-0).
- [7] D.Y. Lee, T.Y. Tseng, Forming-free resistive switching behaviors in Cr-embedded  $\text{Ga}_2\text{O}_3$  thin film memories, *Appl. Phys. Lett.* 110 (2011) 114117, <https://doi.org/10.1063/1.3665871>, 1–114117–5.
- [8] R. Waser, M. Aono, Nanoionics-based resistive switching memories, *Nat. Mater.* 6 (2007) 833–840, <https://doi.org/10.1038/nmat2023>.
- [9] L. Binet, D. Gourier, Optical evidence of intrinsic quantum wells in the transparent conducting oxide  $\beta\text{-Ga}_2\text{O}_3$ , *Appl. Phys. Lett.* 77 (2000) 1138–1140, <https://doi.org/10.1063/1.1289655>.
- [10] D.Y. Guo, Z.P. Wu, Y.H. An, P.G. Li, P.C. Wang, X.L. Chu, X.C. Guo, Y.S. Zhi, M. Lei, L.H. Li, W.H. Tang, Unipolar resistive switching behavior of amorphous gallium oxide thin films for nonvolatile memory applications, *Appl. Phys. Lett.* 106 (2015), 042105, <https://doi.org/10.1063/1.4907174>. –1–042105–5.
- [11] H. Cui, H.F. Mohamed, C. Xia, Q. Sai, W. Zhou, H. Qi, J. Zhao, J. Si, X. Ji, Tuning electrical conductivity of  $\beta\text{-Ga}_2\text{O}_3$  single crystals by Ta doping, *J. Alloys Compd.* 788 (2019) 925–928, <https://doi.org/10.1016/j.jallcom.2019.02.076>.

- [12] F. Alema, Y. Zhang, A. Osinsky, N. Orishchin, N. Valente, A. Mauze, J.S. Speck, Low  $10^{14}$  cm<sup>-3</sup> free carrier concentration in epitaxial  $\beta$ -Ga<sub>2</sub>O<sub>3</sub> grown by MOCVD, *Apl. Mater.* 8 (2020), 021110, <https://doi.org/10.1063/1.5132752>. –1–201110–10.
- [13] J. Zhang, J. Shi, D.C. Qi, L. Chen, K.H.L. Zhang, Recent progress on the electronic structure, defect, and doping properties of Ga<sub>2</sub>O<sub>3</sub>, *Apl. Mater.* 8 (2020), 020906, <https://doi.org/10.1063/1.5142999>. –1–020906–36.
- [14] Z. Liu, Y. Zhi, S. Li, Y. Liu, X. Tang, Z. Yan, P. Li, X. Li, D. Guo, Z. Wu, W. Tang, Comparison of optoelectrical characteristics between Schottky and Ohmic contacts to  $\beta$ -Ga<sub>2</sub>O<sub>3</sub> thin film, *J. Phys. D Appl. Phys.* 53 (2020), 085105, <https://doi.org/10.1088/1361-6463/ab596f>. –1–085105–16.
- [15] T. Shi, R. Wang, Z. Wu, Y. Sun, J. An, Q. Liu, A review of resistive switching devices: performance improvement, characterization, and applications, *Small Struct. B* (2021), 2000109, <https://doi.org/10.1002/ssr.202000109>. –1–2000109–26.
- [16] W. Shen, R. Dittmann, U. Breuer, R. Waser, Improved endurance behavior of resistive switching in (Ba, Sr) TiO<sub>3</sub> thin films with W top electrode, *Appl. Phys. Lett.* 93 (2008), 222102, <https://doi.org/10.1063/1.3039809>. –1–222102–4.
- [17] V.R. Nallagatla, J. Kim, K. Lee, S.C. Chae, C.S. Hwang, C. Uk Jung, Complementary resistive switching and synaptic-like memory behavior in an epitaxial SrFeO<sub>2.5</sub> thin film through oriented oxygen-vacancy channels, *ACS Appl. Mater. Interfaces* 12 (2020) 41740–41748, <https://doi.org/10.1021/acsami.0c10910>.
- [18] B. H Choi, H.B. Im, J.S. Song, K. H Yoon, Optical and electrical properties of Ga<sub>2</sub>O<sub>3</sub>-doped ZnO films prepared by r.f. sputtering, *Thin Solid Films* 193 (1990) 712–720, [https://doi.org/10.1016/0040-6090\(90\)90223-Z](https://doi.org/10.1016/0040-6090(90)90223-Z).
- [19] L. Dong, R. Jia, B. Xin, B. Peng, Y. Zhang, Effects of oxygen vacancies on the structural and optical properties of  $\beta$ -Ga<sub>2</sub>O<sub>3</sub>, *Sci. Rep.* 7 (2017), 40160, <https://doi.org/10.1038/srep40160>, 1–40160–12.
- [20] J.B. Varley, J.R. Weber, A. Janotti, C.G. Van de Walle, Oxygen vacancies and donor impurities in  $\beta$ -Ga<sub>2</sub>O<sub>3</sub>, *Appl. Phys. Lett.* 97 (2010), 142106, <https://doi.org/10.1063/1.3499306>. –1–142106–4.
- [21] J. Montes, C. Kopas, H. Chen, X. Huang, T.H. Yang, K. Fu, C. Yang, J. Zhou, X. Qi, H. Fu, Y. Zhao, Deep level transient spectroscopy investigation of ultra-wide bandgap (2-01) and (001)  $\beta$ -Ga<sub>2</sub>O<sub>3</sub>, *J. Appl. Phys.* 128 (2020), 205701, <https://doi.org/10.1063/5.0021859>. –1–205701–10.
- [22] T. Gu, Role of oxygen vacancies in TiO<sub>2</sub>-based resistive switches, *J. Appl. Phys.* 113 (2013), 033707, <https://doi.org/10.1063/1.4779767>. –1–033707–8.
- [23] Y.S. Lin, F. Zeng, S.G. Tang, H.Y. Liu, C. Chen, S. Gao, Y.G. Wang, F. Pan, Resistive switching mechanisms relating to oxygen vacancies migration in both interfaces in Ti/HfO<sub>x</sub>/Pt memory devices, *J. Appl. Phys.* 113 (2013), 064510, <https://doi.org/10.1063/1.4791695>. –1–064510–6.
- [24] R. Saha, S. Bhowmick, M. Mishra, A. Sengupta, S. Chattopadhyay, S. Chakrabarti, Impact of deposition temperature on crystalline quality, oxygen vacancy, defect modulations and hetero-interfacial properties of RF sputtered deposited Ga<sub>2</sub>O<sub>3</sub> thin films on Si substrate, *J. Phys. D Appl. Phys.* 55 (2022), 505101, <https://doi.org/10.1088/1361-6463/ac9b69>. –1–505101–15.
- [25] A. Mahmoodinezhad, C. Janowitz, F. Naumann, P. Plate, H. Gargouri, K. Henkel, D. Schmeißer, J.I. Flege, Low-temperature growth of gallium oxide thin films by plasma-enhanced atomic layer deposition, *J. Vac. Sci. Technol. A* 38 (2020), 022404, <https://doi.org/10.1116/1.5134800>. –1–022404–12.
- [26] H. Liu, C. Xu, X. Pan, Z. Ye, The photoluminescence properties of  $\beta$ -Ga<sub>2</sub>O<sub>3</sub> thin films, *J. Electron. Mater.* 49 (2020) 4544–4549, <https://doi.org/10.1007/s11664-020-08134-6>.
- [27] S. Ghose, S. Rahman, L. Hong, J.S. Rojas-Ramirez, H. Jin, K. Park, R. Klie, R. Droopad, Growth and characterization of  $\beta$ -Ga<sub>2</sub>O<sub>3</sub> thin films by molecular beam epitaxy for deep-UV photodetectors, *J. Appl. Phys.* 122 (2017), 095302, <https://doi.org/10.1063/1.4985855>, 1–095302–9.
- [28] H. Lim, D. Kim, S.Y. Cha, B.S. Mun, D.Y. Noh, H.C. Kang, Crystallization and bandgap variation of non-stoichiometric amorphous Ga<sub>2</sub>O<sub>3-x</sub> thin films during post-annealing process, *Appl. Surf. Sci.* 585 (2022) 152771, <https://doi.org/10.1016/j.apsusc.2022.152771>, 1–152771–7.
- [29] K. Matsuzaki, H. Hiramatsu, K. Nomura, H. Yanagi, T. Kamiya, M. Hirano, H. Hosono, Growth, structure and carrier transport properties of Ga<sub>2</sub>O<sub>3</sub> epitaxial film examined for transparent field-effect transistor, *Thin Solid Films* 496 (2006) 37–41, <https://doi.org/10.1016/j.tsf.2005.08.187>.
- [30] L. Dong, R. Jia, B. Xin, Y. Zhang, Effects of post-annealing temperature and oxygen concentration during sputtering on the structural and optical properties of  $\beta$ -Ga<sub>2</sub>O<sub>3</sub> films, *J. Vac. Sci. Technol. A* 34 (2016), 060602, <https://doi.org/10.1116/1.4963376>. –1–060602–6.
- [31] K. Takagi, T. Ono, First-principles study on leakage current caused by oxygen vacancies at HfO<sub>2</sub>/SiO<sub>2</sub>/Si interface, *Jpn. J. Appl. Phys.* 57 (2018), 066501, <https://doi.org/10.7567/JJAP.57.066501>. –1–066501–5.
- [32] D. Cui, Y. Du, Z. Lin, M. Kang, Y. Wang, J. Su, J. Zhang, Y. Hao, J. Chang, Coexistence of bipolar and unipolar resistive switching behavior in amorphous Ga<sub>2</sub>O<sub>3</sub> based resistive random access memory device, *IEEE Electron. Device Lett.* 44 (2023) 237–240, <https://doi.org/10.1109/LED.2022.3230247>.
- [33] J.J. Huang, T.C. Chang, J.B. Yang, S.C. Chen, P.C. Yang, Y.T. Chen, H.C. Tseng, S.M. Sze, A.K. Chu, M.J. Tsai, Influence of oxygen concentration on resistance switching characteristics of gallium oxide, *IEEE Electron. Device Lett.* 33 (2012) 1287–1389, <https://doi.org/10.1109/LED.2012.2206365>.
- [34] G. Wang, C. Li, Y. Chen, Y. Xia, D. Wu, Q. Xu, Reversible voltage dependent transition of abnormal and normal bipolar resistive switching, *Sci. Rep.* 6 (2016), 36953, <https://doi.org/10.1038/srep36953>. –1–36953–8.
- [35] D. Cui, Y. Du, Z. Lin, M. Kang, Y. Wang, J. Su, J. Zhang, Y. Hao, Coexistence of bipolar and unipolar resistive switching behavior in amorphous Ga<sub>2</sub>O<sub>3</sub> based resistive random access memory device, *IEEE Electron. Device Lett.* 44 (2023) 237–240, <https://doi.org/10.1109/LED.2022.3230247>.
- [36] C.P. Hsiung, J.Y. Gan, S.H. Tseng, N.H. Tai, P.J. Tzeng, C.H. Lin, F. Chen, M.J. Tsai, Resistance switching characteristics of TiO<sub>2</sub> thin films prepared with reactive sputtering, *Electrochem. Solid State Lett.* 12 (2009) G31, <https://doi.org/10.1149/1.3122742>. –G33.
- [37] N. Wei, X. Ding, S. Gao, W. Wu, Y. Zhao, HfO<sub>x</sub>/Ge RRAM with high ON/OFF ratio and good endurance, *Electronics* 11 (2022) 3820, <https://doi.org/10.3390/electronics11223820>. –1–3820–9.
- [38] F.M. Simanjuntak, D. Panda, K.H. Wie, T.Y. Tseng, Status and prospects of ZnO-based resistive switching memory devices, *Nanoscale Res. Lett.* 11 (2016) 368, <https://doi.org/10.1186/s11671-016-1570-y>, 1–368–31.
- [39] S.J. Park, J.P. Lee, J.S. Jang, H. Rhu, H. Yu, B.Y. You, C.S. Kim, K.J. Kim, Y.J. Cho, S. Baik, In situ control of oxygen vacancies in TiO<sub>2</sub> by atomic layer deposition for resistive switching devices, *Nanotechnology* 24 (2013), 295202, <https://doi.org/10.1088/0957-4484/24/29/295202>. –1–295202–12.
- [40] Y.L. Chung, W.H. Cheng, J.S. Jeng, W.C. Chen, S.A. Jhan, J.S. Chen, Joint contributions of Ag ions and oxygen vacancies to conducting filament evolution of Ag/TaO<sub>x</sub>/Pt memory device, *J. Appl. Phys.* 116 (2014), 164502, <https://doi.org/10.1063/1.4899319>. –1–164502–6.
- [41] W. Wang, B. Zhang, H. Zhao, Forming-free bipolar and unipolar resistive switching behaviors with low operating voltage in Ag/Ti/CeO<sub>2</sub>/Pt devices, *Results Phys.* 16 (2020), 103001, <https://doi.org/10.1016/j.rinp.2020.103001>, 1–103001–5.
- [42] A. Sakic, T.L.M. Scholtes, W.d. Boer, N. Golshani, J. Derakhshandeh, L.K. Nanver, Arsenic-Doped high-resistivity-silicon epitaxial layers for integrating low-capacitance diodes, *Materials* 4 (2011) 2092–2107, <https://doi.org/10.3390/ma4122092>.
- [43] V. Shrotriya, Y. Yang, Capacitance–voltage characterization of polymer light-emitting diodes, *J. Appl. Phys.* 97 (2005), 054504, <https://doi.org/10.1063/1.1857053>. –1–054504–7.
- [44] M.J. Yun, D. Lee, S. Ki, C. Wenger, H.D. Kim, A nonlinear resistive switching behaviors of Ni/HfO<sub>2</sub>/TiN memory structures for self-rectifying resistive switching memory, *Mater. Charact.* 182 (2021) 111578, <https://doi.org/10.1016/j.matchar.2021.111578>, 1–111578–7.
- [45] P. Muhammed Razi, S. Angappane, R.B. Gangineni, Bipolar resistive switching studies in amorphous barium titanate thin films in Ag/am-BTO/ITO capacitor structures, *Mater. Sci. Eng. B* 263 (2021), 114852, <https://doi.org/10.1016/j.mseb.2020.114852>, 1–114852–7.
- [46] M. Liang, L. Wang, V. Presser, X. Dai, F. Yu, J. Ma, Combining battery-type and pseudocapacitive charge storage in Ag/Ti<sub>3</sub>C<sub>2</sub>T<sub>x</sub> MXene electrode for capturing chloride ions with high capacitance and fast ion transport, *Adv. Sci.* (2020), <https://doi.org/10.1002/adv.202000621>, 2000621–1–2000621–9.
- [47] H. Wang, N. Mi, S. Sun, W. Zhang, S. Yao, Oxygen vacancies enhancing capacitance of MgCo<sub>2</sub>O<sub>4</sub> for high performance asymmetric supercapacitors, *J. Alloys Compd.* 869 (2021), <https://doi.org/10.1016/j.jallcom.2021.159294>, 159294–1–159294–8.
- [48] S. Maikap, A. Das, T.Y. Wang, T.C. Tien, L.B. Chang, High- $\kappa$  HfO<sub>2</sub> nanocrystal memory capacitors prepared by phase separation of atomic-layer-deposited HfO<sub>2</sub>/Al<sub>2</sub>O<sub>3</sub> nanomixtures, *J. Electrochem. Soc.* 156 (2009), <https://doi.org/10.1149/1.3070660>, K28–K32.
- [49] S.Z. Rahaman, S. Maikap, T.C. Tien, H.Y. Lee, W.S. Chen, F.T. Chen, M.J. Kao, M.J. Tsai, Excellent resistive memory characteristics and switching mechanism using a Ti nanolayer at the Cu/TaO<sub>x</sub> interface, *Nanoscale Res. Lett.* 7 (2012) 345, <https://doi.org/10.1186/1556-276X-7-345>. –1–345–11.